Dalton Transactions

Accepted Manuscript

ROYAL SOCIETY OF CHEMISTRY

www.rsc.org/dalton

TOC ILLUSTRATION

The reactivity of a series of small size RNAs towards mono-aquated cisplatin was monitored using UV/vis spectroscopy. Subtle changes of local melting behavior of these RNAs were found to influence metal binding kinetics, with an increase in reactivity following central destabilization.

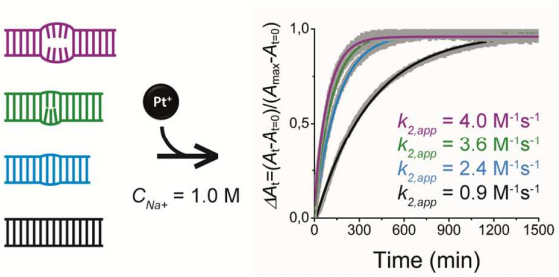

Please note that a high resolution illustration is provided as separate zip-file

RSCPublishing

ARTICLE

Cisplatin-induced duplex dissociation of complementary and destabilized short GG-containing duplex RNAs

Cite this: DOI: 10.1039/x0xx00000x

Received 00th January 2012,
Accepted 00th January 2012

DOI: 10.1039/x0xx00000x

www.rsc.org/

Christopher Polonyi,[a†] Alak Alshiekh,[a†] Lamya A. Sarsam,[b] Maria Clausén,[a] and Sofi K. C. Elmroth[a*]

The ability of the anticancer active drug cisplatin to exert biological activity through interference with nucleic acid function is well documented. Since kinetics play a key role in determining product distributions in these systems, methods for accurate documentation of reactivity serve the purpose to identify preferential metal binding sites. In the present study, the aim has been to further explore a recently communicated approach (C. Polonyi and S. K. C. Elmroth, *J. Chem. Soc., Dalton Trans.*, 2013, **42**, 14959 - 14962) utilizing UV/vis spectroscopy and metal induced duplex RNA melting for monitoring of kinetics. More specifically, the sensitivity of the UV/vis-methodology has been evaluated by investigation of how overall length and changes of base-pairing in the close vicinity of a centrally located GG-site affect the rate of cisplatin binding, using the intracellularly active mono-aquated form of cisplatin (*cis*-$Pt(NH_3)_2Cl(OH_2)^+$, (**1a**)) as the platination reagent. For this purpose, the reactivity of five different 13- to 17 base-pair duplex RNAs was monitored at 38 °C. A common trend of a ca. 10-fold reduction in reactivity was found to accompany an increase of bulk sodium concentration from C_{Na+} = 122 mM to 1.0 M. Typical half-lives are exemplified by the interaction of **1a** with the fully complementary 15-mer RNA-1 with $t_{1/2}$ = ca. 0.5 and 4.8 hours, at C_{Na+} = 122 mM and 1.0 M respectively, and $C_{\mathbf{1a}}$ = 45 μM. Lowering of melting temperature (T_m) was found to promote reactivity regardless of whether the change involved a decrease or increase of the RNA length. For example, at C_{Na+} = 1.0 M, truncation of the fully complementary and GG-containing 15-mer RNA-1 (T_m = 68.9 °C) to the 13-mer RNA-1-1-S (T_m = 63.9 °C) resulted in an increase of $k_{2,app}$ from ca. 0.9 $M^{-1}s^{-1}$ to 2.0 $M^{-1}s^{-1}$. Further, the 17-mer RNA-1-4 (T_m = 42.0 °C) with a central U_4 bulge exhibited the highest reactivity of the sequences studied with $k_{2,app}$= 4.0 $M^{-1}s^{-1}$. The study shows that the reactivity of GG-sequences in RNA exhibit a strong variation depending on exact sequence context, and with imperfectly matched and/or stacked regions as particularly reactive sites.

Introduction

The ability of metal-based coordination compounds to interact and exert biological activity through interactions with nucleic acids is well established.[1-3] Within this research field, studies of the clinically used anticancer drug *cis*-$Pt(NH_3)_2Cl_2$ (cisplatin, *cis*-diamminedichloridoplatinum(II), **1**) constitute a thoroughly explored avenue.[4] In particular, the ability of cisplatin to disrupt nuclear DNA function, together with its downstream biological consequences such as induction of *e.g.* apoptosis and necrosis, has been well documented.[5-7] Despite the high potency of cisplatin against for example testicular-, ovarian- and head- and neck cancers, the need for alternative treatment options and modes of therapeutic interference is higly warranted due to common clinical limitations caused by combination of toxic side effects and resistance development.[8, 9]

From a cellular perspective, adduct formation with nuclear DNA may be regarded as the endpoint for a drug being successfully transported from the extracellular environment, over the cellular membrane, through the cytosol, and finally entering the nucleus. Since RNA share many chemical properties with DNA and is available already in both the cytosol and extracellular environment,[10-13] it seems highly likely that it acts as an effective both kinetic- and thermodynamic scavenger for cisplatin in humans.[14] The ability of RNA to kinetically compete with DNA for cisplatin was first confirmed by model system studies of similar sequence short hairpin DNAs and RNAs.[15] More recently, the ability of

intracellular RNAs to scavenge cisplatin in a site specific manner has been documented in cellular systems by studies of platination patterns on ribosomal RNA (rRNA) from *E. coli* and *S. cerevisiae*.[16, 17] Together, these studies clearly indicate that in addition to DNA-interference, formation of RNA-adducts takes place in the cellular environment, although its effect on biological function in large remains to be investigated.

Among cytosolically located RNAs, the family of microRNAs (miRs) have emerged as one with profound influence on both cellular differentiation and disease development.[11, 18-22] In addition, artificially introduced small duplex RNAs (siRNAs), which for example can be designed to mimic or attenuate the function of endogenous miRs, are today commonly used experimental tools and reaching acceptance as drug candidates and biomarkers.[23-26] Both miRs and siRNAs exert their activity through base-pairing with mRNA in a process facilitated by the RNA induced silencing complex (RISC).[27] Studies in our laboratory has previously shown that platinated siRNAs remain active, however with reduced activity,[28-30] thus in line with cisplatin being able to alter biological function *via* upstream interference with mRNA translation. In a more recent study, we were also able to show that the mature miR-146a readily interacts with the cationic monoaqua metabolite of cisplatin (*cis*-$Pt(NH_3)_2Cl(OH_2)^+$, **1a**) in a reaction that resulted in duplex dissociation at 38 °C.[31] By monitoring the change of absorbance as a function of time, kinetic data was obtained allowing for determination of reaction rate constants for platination of miR-146a together with that of two model systems containing a central either GG- or GUG-binding site. In the current investigation, we now present an extension of this initial study which includes kinetic data for five related RNA sequences, all with a centrally located GG site, see **Scheme 1**. In addition to a variation of the overall lenghts of these RNAs, the influence from variation of central duplex complementarity has been investigated. The central sequence motifs studied are all commonly found in the RNA world and include GU-wobbles (RNA-1-2), a single-base UAU bulge (RNA-1-3), and an extended, mismatched U_4-bulge (RNA-1-4).[32-36] The study shows that first of all, already adduct formation with the monoaqua complex of cisplatin (**1a**) induces structural changes of small RNAs which affects their melting behaviour. Second, a combination of global and local melting properties, rather than overall size, seems to dominate reactivity in these systems.

Experimental

Chemicals and solutions

All oligonucleotides (5´-UU CUU GGU UCU CU-3´ and 5´-AG AGA ACC AAG AA-3´ (RNA-1-1-S), 5´-CUU CUU GGU UCU CUU-3´ and 5´-AAG AGA ACC AAG AAG-3´ (RNA-1), 5´-CUU CUU GGU UCU C-3´ and 5´-GAG AAU UAA GAA G-3´ (RNA-1-2), 5´-CUU CUU GGU UCU CUU-3´ and 5´-AAG AGA AUA UAA GAA G-3´ (RNA-1-3), 5´-UCU UCU UGG UUC UCU UU-3´ and 5´-AAA GAG AUU UUA GAA GA-3´ (RNA-1-4)) were purchased from IBA GmbH (IBA Nucleic Acids Synthesis, Göttingen, Germany) of HPLC grade quality. Cisplatin (*cis*-$Pt(NH_3)_2Cl_2$), (**1**)) and dimethylformamide (DMF) were obtained from Sigma-Aldrich. Sodium dihydrogen phosphate monohydrate ($NaH_2PO_4 \bullet H_2O$), disodium hydrogen phosphate dihydrate ($Na_2HPO_4 \bullet 2H_2O$), sodium perchlorate monohydrate ($NaClO_4 \bullet H_2O$), and silver nitrate ($AgNO_3$) was obtained from Merck. All water used was of Millipore quality and autoclaved before use.

Kinetic studies

A stock soluation of **1** was prepared by addition of 3.9 mg of **1** to 1.30 ml DMF. The solution was vortexed (1400 rpm) over night at room temperature to allow for dissolution. A solution of $AgNO_3$ was prepared by dissolving 2.3 mg $AgNO_3$ in 1.38 ml DMF. Dissolution was obtained after vortexing (2200 rpm) during 5 min at room temperature. Addition of 0.98 mole equivalents of $AgNO_3$ in DMF to the solution of **1** in DMF was made to allow for precipitation of one mole equivalent AgCl (s) and formation of *cis*-$[Pt(NH_3)_2Cl(DMF)^+]$, which upon dissolution in H_2O is rapidly converted to mono-aquated cisplatin (*cis*-$[Pt(NH_3)_2Cl(OH_2)^+]$, (**1a**)), see **Scheme 1**. The mixture was incubated at 37 °C during shaking (170 rpm) for 24 h in the dark. Precipitated AgCl (s) was removed by two consecutive centrifugations (during 3h, and 2 h and 30 min) at room temperature. The supernatant was transferred to Eppendorf tubes after each centrifugation step. Stock solutions of **1a** were stored in a desiccator together with silica gel, and were kept in the dark at room temperature.

Kinetic studies were performed on a Varian Cary 4000 spectrophotometer, equipped with a thermal control unit. Equal concentrations of the (a)- and (b) strands of each duplex RNA-1-1-S, RNA-1, RNA-1-2, RNA-1-3, RNA-1-4 (**Scheme 1**), were mixed separately and the measurements were conducted with a total strand concentration (C_T; $C_T = C_{RNAa} + C_{RNAb}$) of 3.0 μM at two different phosphate buffer (P_i) conditions *i*) C_{Na+} = 122 mM, pH 5.7, and *ii*) C_{Na+} = 1.0 M, pH 5.7. Concentrated stock solutions were prepared according to literature[37] and adjustment of C_{Na+} was made by addition of $NaClO_4$ to buffers (*i*) and (*ii*). The stock solutions were diluted 5-fold (*i.e.* C_{Pi} = 20 mM in buffer (*i*)) and and 2-fold (*i.e.* C_{Pi} = 50 mM in buffer (*ii*)). Prior to measurements, the complementary oligonucleotides were first heated to 90 °C and then allowed to hybridize by slow cooling (0.5 °C/min) to 20 °C. The annealed duplexes were then reheated to 38 °C and **1a** was added. The final concentrations were C_{1a} = 7.5, 15.0, 22.5, 30.0 and 45.0 μM, resulting in ratios $C_{\mathbf{1a}}$:$C_{nucleotide}$ (r_b) in the range of 0.1 – 1.1. The change in absorbance was measured at λ = 260 nm after addition of **1a**.

Thermal melting studies

Thermal melting studies were performed on a Varian Cary 4000 spectrophotometer, equipped with a thermal control unit. The oligonucleotide strands for RNA-1-1-S, RNA-1, RNA-1-2,

RNA-1-3, and RNA-1-4, were mixed separately and the measurements were conducted with C_T = 3.0 μM in buffers (*i*) and (*ii*), see above for detailed description of each buffer. The complementary oligonucleotides were heated to 90 °C and allowed to hybridize by slow cooling (0.5 °C/min) to 20 °C. The temperature was kept at 20 ºC for 5 minutes, followed by heating (0.5 ºC/min) to 90 ºC. The thermal melting points (T_m) were evaluated by the first derivative method, using the Cary WinUV software. Data points were collected every 0.20 °C and the equidistant data was used for the Savitzky-Golay calculations.[38] These calculations give rise to a minimized signal noise, by obtaining a new derivative point out of a determined number of surrounding data points.

Results

Sequences and melting temperatures

In the present study, thermodynamic properties and platinum binding kinetics are reported for a series of 13 - 17-mer duplex RNAs, see **Scheme 1**. The studied sequences have thermodynamic properties in common with the family of short non-coding RNAs, *e.g.* miRs, which are known to be involved in regulation of protein synthesis.[11, 18-22] The present investigation focusses on the properties of five closely related duplexes; RNA-1-1-S, RNA-1, RNA-1-2, RNA-1-3 and RNA-1-4. These RNAs all share sequence motifs with the fully complementary duplex RNA-1, *i.e.* with a common (a)-strand sequence of at least 13 bases containing a centrally located GG-site. Further, the duplexes RNA-1, RNA-1-2, RNA-1-3 and RNA-1-4 represent a series in which the base pairing ability of the GG-site is gradually decreased by modification of the complementary (b)-strand; in RNA-1-2 by mutation of the centrally located complementary CC-sequence for UU, in RNA-1-3 by introduction of the UAU-bulge, and in RNA-1-4 by introduction of a central UUUU-sequence, in the latter case leading to destabilization also of base pairing at sites directly flanking the GG-binding site. Such mismatches and bulges are commonly found *e.g.* in both mature and precursor miRs, and platination of these may interfere with their function in a manner similar to that caused by point-mutations.[22, 39, 40] The overall length of RNA-1-2, -1-3 and -1-4 was adjusted by removal or introduction of terminal AU base pairs to give the sequences RNA-1-2, RNA-1-3, and RNA-1-4 similar melting temperatures, thereby facilitate the reactivity comparison between these three RNA duplexes. Finally, the introduction of a shorter version of the fully complementary sequence by use of RNA-1-1-S was made to enable evaluation of a minor variation of the length and related changes in melting temperature on reactivity.

Experimentally determined melting temperatures (T_m:s) were obtained by analysis of the absorbance change as a function of increasing temperature. The data is summarized in **Table 1** (see methods for details and experimental data in **Figures S1** and **S2**). As can be seen here, the sequences RNA-1-2, RNA-1-3 and RNA-1-4 have melting temperatures close to body temperature at physiologically relevant salt concentration (C_{Na+} = 122 mM), with RNA-1-2 and RNA-1-3 exhibiting the higher $\underline{T_m}$:s at both C_{Na+} = 122 mM and 1.0 M; ca. 39 and 46 °C, respectively. For RNA-1-4 the corresponding data is ca. 36 and 42 °C at C_{Na+} = 122 mM and 1.0 M, respectively. Finally, the T_m:s for the fully complementary 13-mer RNA-1-1-S was determined to ca. 57 and 64 °C at the two salt concentrations employed. Thus, these values are slightly lower compared with the T_m:s for the fully complementary 15-mer duplex RNA-1, but significantly above that of both the similar sized, GU-wobble containing RNA-1-2 and the longer sequences with central mismatches.

Spectral changes induced by addition of 1a

In a recent communication we have described a novel method for evaluation of metal binding to duplex RNA using monoaquated cisplatin (**1a**) as the metalation reagent.[31] In brief, the method relies on the ability of the metal complex to destabilize the duplex and induce melting, and the concomitant hyperchromicity is used to monitor binding.[41] As illustrated in **Figure 1**, the reaction is also accompanied by a ca 3 nm bathochromic shift of the absorbance maximum from ca 259 to 262 nm. Thus, the magnitude of both hyperchromicity and bathochromic shift is similar to previous observations made after binding of cisplatin to DNA.[41-43] The largest change in absorption is obtained for systems where metalation results in conversion of predominant duplex RNAs to metalated single-stranded oligonucleotides, a phenomenon typically observed for RNA-1 when studied at 38 °C. In comparison to the overall absorbance change following melting (**Figure 2A**), the absorbance change induced by metalation constitutes the major component (**Figure 2B**), to which only minor additions of temperature related absorbance changes need to be added to account for the expected ΔA based on melting alone; ΔA related to the temperature change in the interval 20 – 38 °C (**Figure 2C**), and ΔA related to the temperature change in the interval 38 – 90 °C, the latter monitored directly after the kinetic study (**Figure 2D**). Also the absorbance changes in the systems investigated closer to their respective T_m-values, *i.e.* RNA-1-1-S, RNA-1-2, RNA-1-3 and RNA-1-4, are well described by the contributions described above. For RNA-1-2, -1-3, and -1-4, the metal-induced absorbance change is reduced in comparison with RNA-1, as anticipated due to the larger proportion of single-stranded material present at addition of the metal reagent.

Metal-induced kinetics

Reactivity and half-lives at C_{Na+} = 1.0 M

Metal-induced kinetics were studied after addition of **1a** to buffered and temperature equilibrated solutions of preannealed duplex RNAs. Pseudo-first-order conditions with C_{1a} typically in at least 10-fold excess compared with the total RNA-strand concentration (C_T) was used to allow for quantitative determination of observed reaction rate constants (k_{obs}) by a fit of a single-exponential function to the experimentally obtained

ΔA-values ($\Delta A_t = A_t - A_{t=0}$). The standard expression for exponential decay according to Eq. (1)

$$\Delta A_t = \Delta A_\infty (1\text{-exp } (-k_{obs} \cdot t)) \quad (1)$$

was used for determination of k_{obs}, with ΔA_∞ denoting the maximum absorbance difference reached at the end of the studied time interval.

A set of representative kinetic traces, together with the corresponding fitted single-exponential functions, are shown in **Figure 3** for reactions of RNA-1, RNA-1-2, RNA-1-3 and RNA-1-4, all investigated at C_{Na+} = 1.0 M and T = 38 °C (data for RNA-1-1-S in **Figure S2A**). The chosen salt concentration allows for monitoring of the reactions in systems with duplex RNA as dominating fraction, compare **Table 1**. Thus, the kinetic amplitudes are close to the expected absorbance change arising from conversion of duplex RNA to single-stranded oligonucleotides. The larger amplitudes were obtained for RNA-1 and RNA-1-3 (**Figures 3A** and **3C**) for which melting in both cases leads to disruption of 15 stacked base-pairs and an observed ΔA of ca. 0.07 A.U. For RNA-1-2, RNA-1-4 and RNA-1-1-S (**Figures 3B**, **3D**, and **S2A**), somewhat reduced amplitudes were obtained with a common ΔA of ca. 0.05 A.U., all in agreement with the common maximum number of 13-stacked base-pairs to be disrupted in these structures upon melting, compare also **Scheme 2**, and the melting curves in **Figures S1** and **S2**. The data in **Figures 3** and **S2A** further shows that all RNAs exhibit reactivity in the hour-range, but with half-lives ($t_{1/2}$) dependent on the actual sequence. For example, the fully complementary 15-mer RNA-1 has the lowest reactivity with $t_{1/2}$ of ca. 290 min (4.8 h) (**Figure 3A**), whereas both the shorter RNA-1-2 and RNA-1-1-S as well as the similar-sized or longer RNAs with reduced central base complementarity (RNA-1-3 and RNA-1-4) have higher reactivity, here with the shortest $t_{1/2}$ of ca. 64 min exhibited by the 17-mer RNA-1-4 (**Figure 3D**).

Reactivity and half-lives at C_{Na+} = 122 mM

To be able to relate reactivity in the studied systems to *in vivo* conditions, a more extensive study at lower salt concentration was next performed. A temperature of 38 °C was used to allow for comparison with previously reported data,[31] and predictability concerning reactivity *e.g.* in living human cells. With the exception of RNA-1-4, kinetics for all sequences outlined in **Scheme 1** could be monitored using UV/vis spectroscopy under these conditions following addition of **1a**. Representative kinetic traces together with fits of data to single-exponential functions are shown in **Figure 4** (data for RNA-1-1-S in **Figure S2B**). A comparison of these data with the ones obtained at C_{Na+} = 1.0 M shows that the reactivity at C_{Na+} = 122 mM is about one order of magnitude higher, all in line with previous observations of kinetics in related RNA- and DNA systems.[15, 44] For example, at the highest concentration of **1a** employed, $C_{\mathbf{1a}}$ = 45 μM, $t_{1/2}$ is in the minute range; 33 min for RNA-1, 11 min for RNA-1-2, and 8 min for RNA-1-3. The trend of half-lives is however identical to that found at C_{Na+} = 1.0 M, with the fully complementary 15-mer RNA-1 exhibiting the lowest reactivity, and with increasing reactivity as the degree of duplex complementarity in the central region or overall size of the RNA is decreased. Inspection of the amplitudes obtained at this lower salt concentration further shows that only the high-melting RNA-1 (T_m = 61.6 °C) and RNA-1-1-S (T_m = 56.7 °C) reach reaction amplitudes similar to those observed at C_{Na+} = 1.0 M, compare **Figures 3**, **4** and **S2**. The reduction of the amplitudes obtained for RNA-1-2 and -1-3 are in good agreement with the expected reduced proportion of duplex RNAs present prior to addition of **1a** (T_m ca. 39 °C for both), and thus confirms our previous assumption of the monitored reaction being associated with the absorbance change following dissociation of duplex RNAs.

Concentration dependence

The reactivity of RNA-1, RNA-1-1-S, RNA-1-2 and RNA-1-3 was next subjected to a more detailed study by variation of the concentration of added **1a**; 7.5 ≤ $C_{\mathbf{1a}}$ ≤ 45 μM and C_{Na+} = 122 mM, complete dataset and fits are shown in **Figures 4** and **S2B**. As illustrated here, addition of **1a** to the duplex RNAs give rise to kinetic traces that are well described by single-exponential functions. Moreover, when the observed rate constants are plotted as a function of added $C_{\mathbf{1a}}$, a linear dependence is observed, see **Figure 5**. Consequently, the concentration dependence is in agreement with a reaction mechanism in which the bimolecular interaction between **1a** and duplex RNA (dsRNA) constitutes the rate determining step, here with subsequent formation of the corresponding dissociated single-stranded RNAs ($ssRNA_a$–**1a** and $ssRNA_b$) as products, see Eqns. (2 and 3) where $k_{2,app}$ denotes the apparent

$$\text{dsRNA} + \mathbf{1a} \xrightarrow{k_{2,app}} \text{ssRNA}_a - \mathbf{1a} + \text{ssRNA}_b \quad (2)$$

$$k_{obs} = k_{2,app} \cdot C_{\mathbf{1a}} \quad (3)$$

second-order rate constant for formation of the covalent RNA-**1a** adduct. For such reaction model, the second-order rate constant $k_{2,app}$ can thus be directly obtained from the slope of a plot of k_{obs} *vs.* $C_{\mathbf{1a}}$. In the absence of a significant intercept, $k_{2,app}$ can also be obtained directly from Eq. (3) by the relation $k_{2,app} = k_{obs}/C_{\mathbf{1a}}$. A summary of the obtained apparent second-order rate constants is made in **Table 1**. Here, $k_{2,app}$ was obtained by linear regression at C_{Na+} = 122 mM, whereas $k_{2,app}$ at C_{Na+} = 1.0 M was obtained directly by use of Eq. (3) and C_{1a} = 45 μM. The data shows that at C_{Na+} = 122 mM, both RNA-1-2 with the centrally located GU-wobbles, and RNA-1-3 with the UAU-bulge, exhibit pronounced higher reactivity ($k_{2,app}$ = ca. 24 and 30 $M^{-1}s^{-1}$, respectively) compared with the fully complementary sequences RNA-1 and RNA-1-1-S ($k_{2,app}$ = ca. 8 and 11 $M^{-1}s^{-1}$, respectively). By increasing the salt concentration to C_{Na+} = 1.0 M the overall reactivity is reduced for all systems, *vide supra*. However, the same reactivity trend is observed for RNA-1, RNA-1-1-S, RNA-1-2 and RNA-1-3;

with a ca. 3-fold higher reactivity of the latter two ($k_{2,app}$ ca. 2.4 and 3.6 $M^{-1}s^{-1}$, respectively) compared with RNA-1 ($k_{2,app}$ ca. 0.9 $M^{-1}s^{-1}$), and with RNA-1-1-S showing a reactivity intermediate between RNA-1 and RNA-1-2 ($k_{2,app}$ ca. 2.0 $M^{-1}s^{-1}$). At this higher salt concentration, now also RNA-1-4 can be included in the comparison revealing this duplex with the centrally located extended bulge to be the most reactive sequence; $k_{2,app}$ ca. 4.0 $M^{-1}s^{-1}$.

Influence of RNA duplex properties on kinetics

A summary of key structural features of the studied RNAs together with their melting properties and reaction rate constants, is made in **Scheme 2**.[45, 46] As can be seen here, the fully complementary 15-mer RNA-1 exhibits the lowest reactivity of all duplexes studied. An influence from overall length and thermal stability on reactivity is revealed for example by a comparison of RNA-1 with the 13-mer RNA-1-1-S. Here, truncation of the duplex by two terminal bases leads to a moderate decrease of T_m (from 68.9 to 63.9 °C) but a significant ca. 2.5-fold increase in reactivity (from 0.88 to 2.02 $M^{-1}s^{-1}$). This observation suggests that the effect on kinetics related to duplex destabilization dominates over the tentative decrease in cation accumulation tendency caused by shortening of the duplex.[44, 47] The influence from destabilization alone is further illustrated by comparison of the similar sized RNA-1-1-S and RNA-1-2. As revealed by the ca. 18 °C lower T_m exhibited by RNA-1-2 compared to RNA-1-1-S, replacement of the central Watson Crick base-pairs for two GU-wobbles causes substantial destabilization of the duplex. The resulting increase in reactivity is relatively modest however; from 2.02 to 2.36 $M^{-1}s^{-1}$, possibly reflecting the similar structures exhibited by these RNAs. Further support for local structure, rather than overall size, as a strong determinant of reactivity is given by a comparison of the similar sized 15-mers RNA-1 and RNA-1-3. Here, disruption of base-pairing by introduction of the single-base mismatch in RNA-1-3 leads to a ca. 23 °C decrease of T_m and a ca. 4-fold increase in reactivity with $k_{2,app}$(RNA-1-3) = 3.64 $M^{-1}s^{-1}$. By further destabilization of the duplex using the central bulge in the 17-mer RNA-1-4 (T_m = 42.0 °C) the reactivity is again increased. It should be noted that the reactivity of RNA-1-4 is significantly above that of both RNA-1-1-S and RNA-1-2 despite the same total number of 13 stacked base-pairs in these RNAs, thus stressing the influence of local duplex properties on reactivity. Finally, a comparison between the two duplexes with similar T_m:s (RNA-1-3 and RNA-1-2) shows that even for systems with identical global melting properties, sequence dependent reactivity can be observed, and with the non-continuously stacked duplex exhibiting the higher reactivity. Together, these data illustrate that first of all, the method of using duplex dissociation as a tool for monitoring RNA reactivity allows for detection of subtle reactivity differences between structures of similar overall composition. Second, the data reveals a dominating influence from melting properties on reactivity, and with disruption of helical stacking as a parameter promoting reactivity, also when either the total number of stacked base-pairs or melting temperature is kept constant.

Discussion

Influence of bulk salt and target type on binding kinetics

The ability of cisplatin to undergo adduct formation reactions with nucleic acids is well established. So far, the majority of kinetic studies reported concern the interaction with DNAs of various sizes, ranging from model systems encompassing the individual nucleobases to extended DNA systems and plasmids.[5, 7, 48-50] As obvious from these studies, several factors are of influence on the adduct formation rates. In addition to the pH- and chloride ion dependent reactivity exhibited by the metal complex itself, the nature of the donor-group and its accessibility in nucleic acid environment is known to be of profound influence on the adduct distribution profile. Further, by systematic studies of the reactivity in small oligomeric DNAs, it has previously been demonstrated that the kinetics for the adduct formation process are strongly dependent on both concentration and type of bulk electrolyte cations, as well as precise location of tentative binding sites within these oligomers.[44] The latter observations agree well with a reaction model in which the oligoelectrolyte properties contribute to facilitate adduct formation by attraction of the cationic mono-aquated cisplatin to the DNA surface.[47, 51] The effect is particularly pronounced for small oligomers up to ca. 15 bases, but seems thereafter to reach a saturation level.[44] Thus, these observations seem to suggest that many of the recently identified small-size intracellular RNAs may be as effective kinetic scavengers for platinum-based drugs as extended DNA *in vivo*.

As an extension of our preliminary report,[31] we here present kinetic data that allows for a detailed comparison between adduct formation rates in helical RNA duplexes and already established trends in similar-size DNA-systems, focusing on adduct formation with RNAs containing centrally located consecutive guanines (GG-site). Our currently reported salt-dependence shows characteristics similar to those previously reported for DNA systems,[15, 44] *i.e.* with kinetically favoured adduct formation rates under low salt conditions (compare **Table 1**), about an order of magnitude increase in reactivity following a decrease of C_{Na+} from ca. 1 M to 100 mM, and a further increase by ca. 3- to 7-fold after lowering the salt concentration to ca. 20 – 30 mM. Over the whole salt interval, the second-order rate constants are comparable to previously reported ones for similar-size nucleic acid systems, but with a noticeable tendency for increased reactivity in our here studied RNAs compared with similar sized DNAs. For example, the reactivity of the fully complementary RNAs and miR-146a ($k_{2,app}$ ca. 20 $M^{-1}s^{-1}$ at C_{Na+} = 22 mM[31]) is significantly above that obtained for adduct formation with *i*) single-stranded 17-mer DNAs ($k_{2,app}$ ca. 7 $M^{-1}s^{-1}$ at C_{Na+} = 35 mM, recalculated from ref. 44) as well as *ii*) interaction with the loop region of a 13-mer hairpin RNA ($k_{2,app}$ ca. 6 $M^{-1}s^{-1}$ at C_{Na+} = 35 mM, ref. 15). Also at C_{Na+} ca. 100 mM, a tendency for increased reactivity of the currently used RNAs can be noticed,

compare for example with previous studies of 22-mer DNA hairpins. More specifically, at C_{Na+} = 122 mM we here observe second-order rate constants ranging from ca. 8 to 30 $M^{-1}s^{-1}$, whereas the reported second-order rate constants for similar size DNA systems are in the range of 0.1 – 0.54 $M^{-1}s^{-1}$.[52, 53] In summary, we can conclude that on a qualitative scale, the RNA duplexes studied exhibit a salt dependence in good agreement with already published studies of similar-size DNA systems, but show a tendency towards increased reactivity when compared to single-stranded and hairpin DNAs of similar size.

Influence of sequence on cisplatin binding kinetics

In extended DNA, cisplatin exhibits a well documented preference for adduct formation with G-N7, with the 1,2-d(GpG) intrastrand cross-link as the preferred adduct type strongly dominating over for example the amount of d(ApG)- and d(GpA) cross-links.[54] As concluded in the review by Kozelka,[49] the DNA sequence selectivity is likely a result of combined contributions of kinetics and thermodynamics; the former influencing initial mono-functional adduct formation and the latter one determining the stability of the bi-functional, and irreversibly bound platinum adduct. In the structurally diverse RNA environment,[55] it seems likely that cisplatin adduct formation may exhibit an even more pronounced sequence dependence compared with DNA, both with respect to binding kinetics and location of thermodynamically stable adducts. Previous studies indicative of such sequence influence includes for example platination of full length- and truncated models of the stem region of $tRNA^{Ala}$.[56, 57] In these systems, preferential platination of G-N7 of the stem region of full length $tRNA^{Ala}$ was found to occur.[57] Detailed model system studies revealed that this interaction required the presence of a GU-wobble base pair.[56] Consequently, platination could be prevented by closure of the wobble by mutation of the GU- to a GC base-pair. Additional studies illustrating the ability of cisplatin to preferentially undergo adduct formation with solvent exposed G-N7 in RNA regions with lower thermal stability include for example the previously mentioned model system studies of short 13-mer hairpins,[15] and interactions with both ribosomal RNA (rRNA),[16, 17] and model systems of spliceosomal U2:U6 RNAs.[58] Together, these studies show that also extended and folded duplex RNAs are platinated during the same time frame as typically used for effective DNA platination,[59] however resulting in more diverse adduct types. In RNA, a large fraction of adducts are typically localized in, or in close proximity to, loop and bulge regions. Due to the structural constraints that are likely to be introduced during formation of the bifunctional adduct,[60, 61] we have speculated the altered adduct profile in RNA may partially reflect local sequence composition – and thus melting behaviour – of the polymer, for example with low-melting regions as particularly prone to react. Our present data is well in line with this speculation. For example, at C_{Na+} = 1.0 M the second-order rate constants increase gradually with decreasing thermodynamic stability around the central GG-binding site despite similar global melting temperatures for RNA-1-2 and RNA-1-3; $k_{2,app}$ = 0.88 $M^{-1}s^{-1}$ (RNA-1), 2.4 $M^{-1}s^{-1}$ (RNA-1-2), 3.6 $M^{-1}s^{-1}$ (RNA-1-3), and 4.0 $M^{-1}s^{-1}$ (RNA-1-4). It should be noted that the difference in reactivity between the fully complementary RNA-1 and both the single- and extended bulge containing RNAs (RNA-1-3 and RNA-1-4) is large enough to allow for selective metalation of both RNA-1-3 and RNA-1-4 in the presence of competing RNA-1. As mismatches are commonly found in the RNA world, this might have an impact on the metalation patterns also in a biological context, since inspection of our available data at physiologically relevant salt concentration (C_{Na+} = 122 mM) reveals the trend to remain also here. We therefore conclude that platination of RNA likely exhibits distinct, but different in comparison to DNA, adduct profile patterns *in vivo*, and with local melting properties as a contributing factor to sequence selectivity.

Conclusions

In the present study we have further explored the use of a UV/vis based approach utilizing duplex RNA dissociation as an indirect method of monitoring platinum-RNA adduct formation.[31, 41-43] Our focus has here been to compare reactivity in systems of relevance for naturally occurring short non-coding RNAs. The approach was shown to provide high quality kinetic data for the interactions of monoaquated cisplatin, **1a**, with duplex RNAs of varying stability; 36 °C < T_m < 69 °C. The kinetics determined at 38 °C for duplexes varying from 13- to 17-mers exhibited pronounced salt dependence. Similar reactivity trends were observed at both high and low salt concentrations however, with typical halv-lives in the minute range at physiologically relevant salt concentrations (C_{Na+} = 122 mM), and in the hour-range at high salt conditions (C_{Na+} = 1.0 M). The second-order rate constants ($k_{2,app}$) were shown to depend on the global melting temperature, with increasing rate constants typically following a decrease in T_m. For example, lowering of T_m from ca. 69 °C in the fully complementary RNA-1 to ca 46 °C in RNA-1-3 by replacement of the central CC-sequence for UAU resulted in an increase of $k_{2,app}$ from 0.88 to 3.64 $M^{-1}s^{-1}$. A more subtle variation in reactivity could also be observed for RNAs with similar T_m:s, indicative of central disruption of duplex stacking as a parameter promoting reactivity. The study implies that already binding of the mono-aquated intermediate of cisplatin has a profound influence on RNA stability *in vivo*, leading to severe disruption of duplex stability, and with consecutive GG-sequences in regions with imperfect base-pairing and/or stacking as the more reactive sites.

Acknowledgements

Financial support from Forskarskolan i Läkemedelsvetenskap (FLÄK) at Lund University, Kungliga Fysiografiska Sällskapet i Lund, Crafoordska Stiftelsen och Cancerfonden is gratefully acknowledged.

Notes and references

[a] Biochemistry and Structural Biology, KILU, Lund University, POBox 124, SE-221 00 Lund, Sweden.
[b] Current address: Department of Chemistry, College of Science, Mosul University, Mosul, Iraq.
[†]These authors contributed equally to the study.

Electronic Supplementary Information (ESI) available: Thermal melting curves at C_{Na+} = 122 mM and 1.0 M for RNA-1-1-S, RNA-1, RNA-1-2, RNA-1-3 and RNA-1-4 and kinetic traces for RNA-1-1-S. See DOI: 10.1039/b000000x/

1 Citations here in the format A. Name, B. Name and C. Name, *Journal Title*, 2000, **35**, 3523; A. Name, B. Name and C. Name, *Journal Title*, 2000, **35**, 3523.

1 A. M. Pizarro and P. J. Sadler, *RSC Biomol. Sci.*, 2009, 350-416.
2 J. Reedijk, *Eur. J. Inorg. Chem.*, 2009, 1303-1312.
3 B. Lippert, *RSC Biomol. Sci.*, 2009, 39-74.
4 B. Rosenberg, L. VanCamp, J. E. Trosko and V. H. Mansour, *Nature*, 1969, **222**, 385-386.
5 K. Cheung-Ong, G. Giaever and C. Nislow, *Chem. Biol.*, 2013, **20**, 648-659.
6 L. Kelland, *Nat. Rev. Cancer*, 2007, **7**, 573-584.
7 Y. Jung and S. J. Lippard, *Chem. Rev.*, 2007, **107**, 1387-1407.
8 B. Köberle, M. T. Tomicic, S. Usanova and B. Kaina, *Biochim. Biophys. Acta*, 2010, **1806**, 172-182.
9 S. M. Sancho-Martinez, L. Prieto-Garcia, M. Prieto, J. M. Lopez-Novoa and F. J. Lopez-Hernandez, *Pharmacol. Ther.*, 2012, **136**, 35-55.
10 M. S. Rodriguez, C. Dargemont and F. Stutz, *Biol. Cell*, 2004, **96**, 639-655.
11 Y. Wang, H. M. Stricker, D. Gou and L. Liu, *Front. Biosci.*, 2007, **12**, 2316-2329.
12 E. E. Creemers, A. J. Tijsen and Y. M. Pinto, *Circul. Res.*, 2012, **110**, 483-495.
13 S. Principe, A. B.-Y. Hui, J. Bruce, A. Sinha, F.-F. Liu and T. Kislinger, *Proteomics*, 2013, **13**, 1608-1623.
14 M. Akaboshi, K. Kawai, H. Maki, K. Akuta, Y. Ujeno and T. Miyahara, *Jap. J. Cancer Res.*, 1992, **83**, 522-526.
15 M. Hagerlof, P. Papsai, C. S. Chow and S. K. C. Elmroth, *J. Biol. Inorg. Chem.*, 2006, **11**, 974-990.
16 K. Rijal and C. S. Chow, *Chem. Commun.*, 2009, 107-109.
17 A. A. Hostetter, M. F. Osborn and V. J. DeRose, *ACS Chem. Biol.*, 2012, **7**, 218-225.
18 R. C. Lee, R. L. Feinbaum and V. Ambros, *Cell*, 1993, **75**, 843-854.
19 V. Ambros, *Nature*, 2004, **431**, 350-355.
20 S. Volinia, G. A. Calin, C. G. Liu, S. Ambs, A. Cimmino, F. Petrocca, R. Visone, M. Iorio, C. Roldo, M. Ferracin, R. L. Prueitt, N. Yanaihara, G. Lanza, A. Scarpa, A. Vecchione, M. Negrini, C. C. Harris and C. M. Croce, *Proc. Natl. Acad. Sci. U. S. A.*, 2006, **103**, 2257-2261.
21 A. N. Gargalionis and E. K. Basdra, *Curr. Top. Med. Chem.*, 2013, **13**, 1493-1502.
22 A. Lujambio and S. W. Lowe, *Nature*, 2012, **482**, 347-355.
23 J. W. Engels, *New Biotechnol.*, 2013, **30**, 302-307.
24 A. Reynolds, D. Leake, Q. Boese, S. Scaringe, W. S. Marshall and A. Khvorova, *Nat. Biotechnol.*, 2004, **22**, 326-330.
25 A. G. Bader, D. Brown and M. Winkler, *Cancer Res.*, 2010, **70**, 7027-7030.
26 N. Hauptman and D. Glavac, *Radiology and Oncology*, 2013, **47**, 311-318.
27 E. F. Finnegan and A. E. Pasquinelli, *Crit. Rev. Biochem. Mol. Biol.*, 2013, **48**, 51-68.
28 M. Hägerlöf, H. Hedman and S. K. C. Elmroth, *Biochem. Biophys. Res. Commun.*, 2007, **361**, 14-19.
29 A. S. Snygg and S. K. C. Elmroth, *Biochem. Biophys. Res. Commun.*, 2009, **379**, 186-190.
30 H. K. Hedman, F. Kirpekar and S. K. C. Elmroth, *J. Am. Chem. Soc.*, 2011, **133**, 11977-11984.
31 C. Polonyi and S. K. C. Elmroth, *J. Chem. Soc., Dalton Trans.*, 2013, **42**, 14959-14962.
32 A. Kozomara and S. Griffiths-Jones, *Nucleic Acids Res.*, 2011, **39**, D152-D157.
33 D. A. Peattie, S. Douthwaite, R. A. Garrett and H. F. Noller, *Proc. Natl. Acad. Sci. USA*, 1981, **78**, 7331-7335.
34 R. R. Gutell, J. J. Cannone, Z. Shang, Y. Du and M. J. Serra, *J. Mol. Biol.*, 2000, **304**, 335-354.
35 P. Dua, J. W. Yoo, S. Kim and D. K. Lee, *Mol. Ther.*, 2011, **19**, 1676-1687.
36 S. Althoff, D. Selinger and J. A. Wise, *Nucleic Acids Res.*, 1994, **22**, 1933-1947.
37 D. D. Moore, *Curr. Protoc. Mol. Biol.*, 2001, 35:A.2.1 - A.2.8.
38 A. Savitzky and M. J. E. Golay, *Anal. Chem.*, 1964, **36**, 1627-1639.
39 B. P. Davies and C. Arenz, *Biorg. Med. Chem.*, 2008, **16**, 49-55.
40 N. Iwai and H. Naraba, *Biochem. Biophys. Res. Commun.*, 2005, **331**, 1439-1444.
41 P. Horacek and J. Drobnik, *Biochim. Biophys. Acta*, 1971, **254**, 341-347.
42 J. P. Macquet and J. L. Butour, *Biochimie*, 1978, **60**, 901-914.
43 H. C. Harder, *Chem.-Biol. Interact.*, 1975, **10**, 27-39.
44 A. S. Snygg, M. Brindell, G. Stochel and S. K. C. Elmroth, *J. Chem. Soc., Dalton Trans.*, 2005, 1221-1227.
45 A. R. Gruber, R. Lorenz, S. H. Bernhart, R. Neuboeck and I. L. Hofacker, *Nucleic Acids Res.*, 2008, **36**, W70-W74.
46 The "RNAfold" program was used to obtain minimum free energy (MFE) secondary strucutres after attachement of a U_5 sequence between the 3´-end of the (a)-strand and the 5´-end of the (b)-strand.
47 M. C. Olmsted, C. F. Anderson and M. T. Record, *Proc. Natl. Acad. Sci. U. S. A.*, 1989, **86**, 7766-7770.
48 J. Arpalahti, *Metal Ions in Biological Systems, Vol 32*, 1996, **32**, 379-395.
49 J. Kozelka, *Inorg. Chim. Acta*, 2009, **362**, 651-668.
50 E. G. Chapman, A. A. Hostetter, M. F. Osborn, A. L. Miller and V. J. DeRose, *Metal Ions in Biological Systems, Vol 32*, 2011, **9**, 347-377.
51 S. K. C. Elmroth and S. J. Lippard, *Inorganic Chemistry*, 1995, **34**, 5234-5243.
52 S. J. Berners-Price, K. J. Barnham, U. Frey and P. J. Sadler, *Chemistry-a European Journal*, 1996, **2**, 1283-1291.

53 V. Monjardet-Bas, S. Bombard, J. C. Chottard and M. Kozelka, *Chem. Eur. J.*, 2003, **9**, 4739-4745.
54 A. M. J. Fichtinger-Schepman, J. L. van der Veer, J. H. J. den Hartog, P. H. M. Lohman and J. Reedijk, *Biochemistry*, 1985, **24**, 707-713.
55 D. E. Draper, D. Grilley and A. M. Soto, *Annu. Rev. Biophys. Biomolec. Struct.*, 2005, **34**, 221-243.
56 P. Papsai, J. Aldag, T. Persson and S. K. C. Elmroth, *J. Chem. Soc., Dalton Trans.*, 2006, 3515-3517.
57 P. Papsai, A. S. Snygg, J. Aldag and S. K. C. Elmroth, *Dalton Transactions*, 2008, 5225-5234.
58 A. A. Hostetter, E. G. Chapman and V. J. DeRose, *J. Am. Chem. Soc.*, 2009, **131**, 9250-9257.
59 M. V. Keck, *J. Chem. Educ.*, 2000, **77**, 1471-1473.
60 J. H. J. den Hartog, C. Altona, J. H. van Boom, G. A. van der Marel, C. A. G. Haasnoot and J. Reedijk, *J. Biomol. Struct. Dyn.*, 1985, **2**, 1137-1155.
61 P. M. Takahara, A. C. Rosenzweig, C. A. Frederick and S. J. Lippard, *Nature*, 1995, **377**, 649-652.

Table 1. Summary of melting temperatures (T_m) and reaction rate constants (k_{obs} and $k_{2,app}$) for RNA-1, RNA-1-1-S, RNA-1-2, RNA-1-3, RNA-1-4.[a]

Duplex	T_m[b] (°C)	$10^4 \times k_{obs}$[c] (s^{-1}) C_{Pt} = 45 µM	$k_{2,app}$[d] ($M^{-1}s^{-1}$)	Reference
C_{Na+} = 122 mM				
RNA-1	61.6 ± 0.2	3.5 ± 0.1	7.7 ± 0.5	*This work*, 30
RNA-1-1-S	56.7 ± 0.1	5.6 ± 0.5	10.5 ± 0.6	*This work*
RNA-1-2	39.6 ± 0.3	11 ± 0.2	23.6 ± 1.0	*This work*
RNA-1-3	39.2 ± 0.1	14 ± 0.3	29.7 ± 1.1	*This work*
RNA-1-4	36.2 ± 0.2	-	*> 30*	*n.d.*[e]
C_{Na+} = 1.0 M				
RNA-1	68.9 ± 0.3	0.40 ± 0.004	0.88 ± 0.11	*This work*
RNA-1-1-S	63.9 ± 0.3	0.93 ± 0.025	2.02 ± 0.05	*This work*
RNA-1-2	46.4 ± 0.2	1.1 ± 0.003	2.36 ± 0.05	*This work*
RNA-1-3	45.9 ± 0.1	1.6 ± 0.005	3.64 ± 0.48	*This work*
RNA-1-4	42.0 ± 0.3	1.8 ± 0.007	4.02 ± 0.07	*This work*

[a] C_T = 3.0 µM. [b] Measurements performed in triplicates. Indicated errors correspond to the standard deviation. [c] Indicated errors for k_{obs} correspond to the largest standard error obtained for the curve fit. [d] Indicated errors for $k_{2,app}$ at C_{Na+} = 122 mM correspond to the standard error of the linear curve fit based on data points from five separate measurements; 7.5 µM < C_{Pt} < 45 µM. Indicated errors for $k_{2,app}$ at C_{Na+} = 1.0 M correspond to the standard error of triplicate data points with C_{Pt} = 45 µM , [e] Reaction over within mixing time.

SCHEMES and FIGURES

Cisplatin-induced duplex dissociation of complementary and destabilized short GG-containing duplex RNAs

Christopher Polonyi,[a] Alak Alshiekh,[a] Lamya A. Sarsam,[b] Maria Clausén,[a] and Sofi K. C. Elmroth[a*]

PLEASE NOTE!
These illustrations are provided as orientation only.
High-resolution illustrations are supplied as separate zip-files.

RNA-1	5′-CUU CUU GGU UCU CUU-3′	(a)
	3′-GAA GAA CCA AGA GAA-5′	(b)
RNA-1-1-S	5′-UU CUU GGU UCU CU-3′	(a)
	3′-AA GAA CCA AGA GA-5′	(b)
RNA-1-2	5′-CUU CUU GGU UCU C-3′	(a)
	3′-GAA GAA UUA AGA G-5′	(b)
RNA-1-3	5′-CUU CUU G GU UCU CUU-3′	(a)
	3′-GAA GAA UAUA AGA GAA-5′	(b)
RNA-1-4	5′-UCUU CUU GGU UCU CUUU-3′	(a)
	3′-AGAA GAU UUU AGA GAAA-5′	(b)

1a

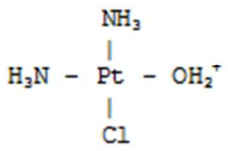

Scheme 1. Schematic illustration of RNA sequences studied and mono-aquated cisplatin (**1a**).

Central basepairing	~UGGU~ |••| ~AUUA~	~UGGU~ |||| ~ACCA~	~UGGU~ |||| ~ACCA~	~UG GU~ || || ~AUAUA~	~U^{GG}U~ ~U$_{UU}$U~
Duplex	RNA-1-2	RNA-1-1-S	RNA-1	RNA-1-3	RNA-1-4
Length	13	13	15	15	17
Stacked bp:s	13	13	15	8+7	7+6
T_m (°C)[a]	46.4	63.9	68.9	45.9	42.0
$k_{2,app}$ ($M^{-1}s^{-1}$)[a]	2.36	2.02	0.88	3.64	4.02

Scheme 2. Illustration of hydrogen bonding patterns surrounding the common central GG sequence together with a summary of the length of the GG-containing strand, number of consecuitvely stacked basepairs obtained after energy minimization,[45,46] melting temperature and the second-order rate constant. [a] C_{Na+} = 1.0 M.

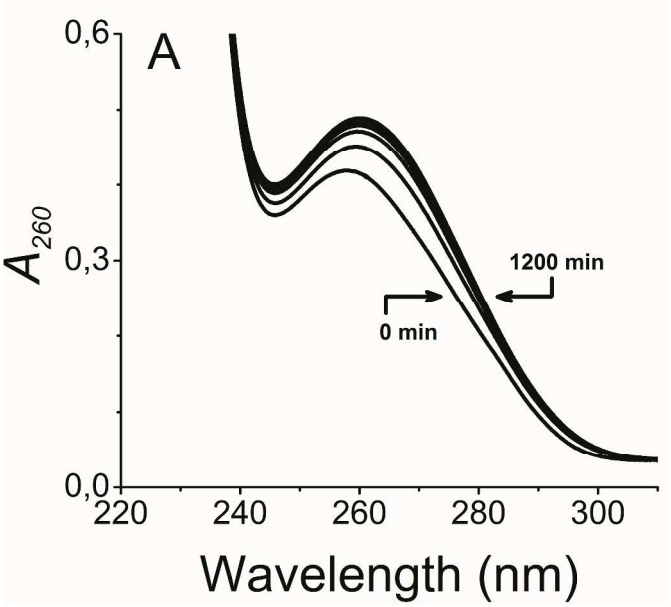

Figure 1. Spectral change as a function of time after addition of **1a** to RNA-1; C_{1a} = 7.5 μM, C_T = 3.0 μM, T = 38 °C, buffered solution; C_{Na+} = 122 mM (20 mM Na_2HPO_4/NaH_2PO_4 pH 5.7, supplemented with 100 mM $NaClO_4$). Spectra were recorded with 200 min interval.

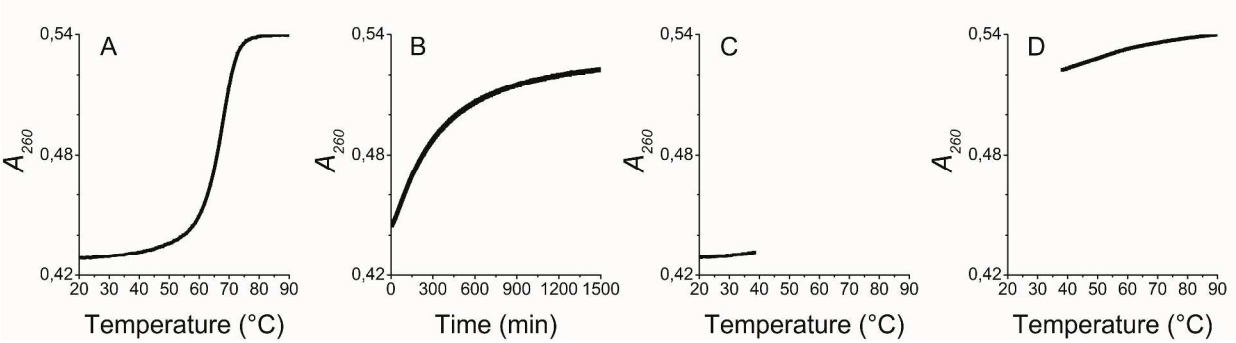

Figure 2. Absorbance change as a function of temperature and time: (A) RNA-1 melting curve, (B) absorbance change as a function of time after addition of **1a** to RNA-1 followed at λ = 260 nm (T = 38 °C and C_{1a} = 45.0 μM), (C) RNA-1 partial melting curve in the interval 20 – 38 °C and (D) RNA-1 partial melting curve in the interval 38 – 90 °C directly following exposure to **1a**, as illustrated in (B). All measurements were conducted with C_T = 3.0 μM in buffered solution; C_{Na+} = 1.0 M (50 mM Na_2HPO_4/NaH_2PO_4 pH 5.7, supplemented with 946 mM $NaClO_4$).

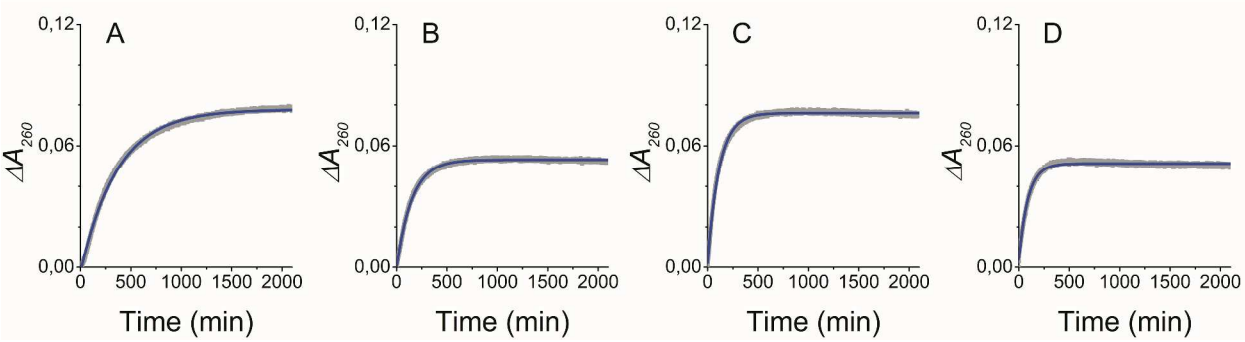

Figure 3. Absorbance change as a function of time after addition of **1a** to (A) RNA-1, (B) RNA-1-2, (C) RNA-1-3 and (D) RNA-1-4. All measurements were conducted with $C_{\boldsymbol{1a}}$ = 45.0 μM, C_T = 3.0 μM and T = 38 °C in buffered solution; C_{Na+} = 1.0 M (50 mM Na_2HPO_4/NaH_2PO_4 pH 5.7, supplemented with 946 mM $NaClO_4$). Fits of a single-exponential function to the experimental data is indicated with a solid line (blue).

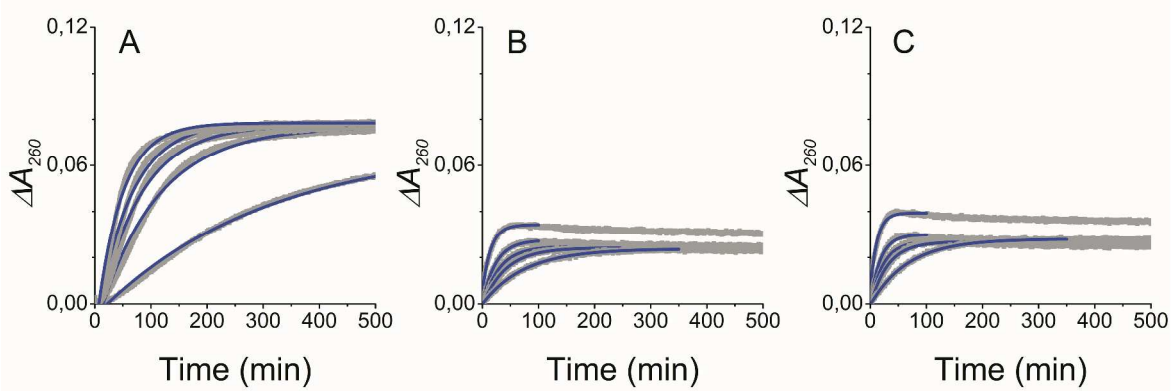

Figure 4. Absorbance change as a function of time together with fits of a single-exponential function to experimental data (blue lines) after addition of **1a** to (A) RNA-1, (B) RNA-1-2 and (C) RNA-1-3. All measurements were conducted with C_{1a} = 7.5 - 45.0 µM, C_T = 3.0 µM and T = 38 °C in buffered solution; C_{Na+} = 122 mM (20 mM Na_2HPO_4/NaH_2PO_4 pH 5.7, supplemented with 100 mM $NaClO_4$).

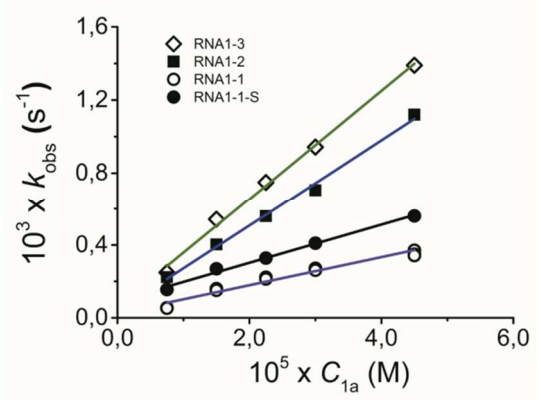

Figure 5. Observed pseudo-first-order rate constants (k_{obs}) plotted as a function of C_{1a} in the interval 7.5 - 45.0 μM together with linear regression lines allowing for determination of $k_{2,app}$ from the slope; (○) RNA-1, (●) RNA-1-1-S, (■) RNA-1-2, and (◊) RNA-1-3. All measurements were conducted in triplicates with C_T = 3.0 μM and C_{Na+} = 122 mM (20 mM Na_2HPO_4/NaH_2PO_4 pH 5.7, supplemented with 100 mM $NaClO_4$).